vehicles

MDPI

Article

Thermal Management of Lithium-Ion Battery Pack Using Equivalent Circuit Model

Muthukrishnan Kaliaperumal and Ramesh Kumar Chidambaram *

Automotive Research Center, Vellore Institute of Technology, Vellore 632014, India; muthukrishnan.k2015@vit.ac.in
* Correspondence: crameshkumar@vit.ac.in

Abstract: The design of an efficient thermal management system for a lithium-ion battery pack hinges on a deep understanding of the cells' thermal behavior. This understanding can be gained through theoretical or experimental methods. While the theoretical study of the cells using electrochemical and numerical methods requires expensive computing facilities and time, the Equivalent Circuit Model (ECM) offers a more direct approach. However, upfront experimental cell characterization is needed to determine the ECM parameters. In this study, the behavior of a cell is characterized experimentally, and the results are used to build a second-order equivalent electrical circuit model of the cell. This model is then integrated with the cooling system of the battery pack for effective thermal management. The Equivalent Circuit Model estimates the internal heat generation inside the cell using instantaneous load current, terminal voltage, and temperature data. By extrapolating the heat generation data of a single cell, we can determine the heat generation of the cells in the pack. With the implementation of the ECM in the cooling system, the coolant flow rate can be adjusted to ensure the attainment of a safe operating cell temperature. Our study confirms that 14% of pumping power can be reduced when compared to the conventional constant flow rate cooling system, while still maintaining the temperature of the cells within safe limits.

Keywords: lithium-ion battery; equivalent circuit model; battery parameters; heat generation; thermal management; SoC

check for updates

Citation: Kaliaperumal, M.; Chidambaram, R.K. Thermal Management of Lithium-Ion Battery Pack Using Equivalent Circuit Model. *Vehicles* **2024**, *6*, 1200–1215. https://doi.org/10.3390/vehicles6030057

Academic Editor: Mohammed Chadli

Received: 26 April 2024
Revised: 5 July 2024
Accepted: 9 July 2024
Published: 11 July 2024

Copyright: © 2024 by the authors. Licensee MDPI, Basel, Switzerland. This article is an open access article distributed under the terms and conditions of the Creative Commons Attribution (CC BY) license (https://creativecommons.org/licenses/by/4.0/).

1. Introduction

The global increase in dependency on fossil fuels has impacted the environment on an extensive basis. Emissions from vehicles and their side effects on humans and nature were pressing issues that made the world consider substitutes for fossil fuels. The automotive sector is slowly marching towards Hybrid Electric Vehicles (HEVs) and pure Electric Vehicle Technologies [1]. Lithium-ion batteries (LIBs), among several types of electrochemical storage devices, are extensively utilized in EVs, HEVs, and other electrical devices. Today, the LIB dominates the battery market due to the benefits of higher energy density, higher specific energy over other rechargeable battery technologies, low self-discharge rate, extended life service, and high cell voltage [2,3]. However, when the LIBs are manufactured, there are differences in the cells' internal resistance, voltage, and capacity [4], and as a result, when cells undergo charging/discharging, it creates uneven temperature [5,6]. The manufacturing tolerances, defects (uneven electrode material deposition), and internal short circuits (due to lithium plating) may create hot spots inside the cells, leading to overheating and thermal runaway [7]. Battery pack failure or thermal runaway leading to vehicle fire is inevitable if the temperature of such cells/battery pack modules is not controlled within the safe operating range. Battery pack failure or thermal runaway leading to vehicle fire is inevitable if the temperature of such cells/battery pack modules is not controlled within the safe operating range. Therefore, battery temperature is critical to the LIB battery module's functionality and safety. Experimental and numerical simulation methods are extensively

used to understand the thermal behavior of the cells at various loads and environmental conditions. Though it is expensive and time-consuming, the experimental approach has its limitations in measuring cell temperature inside the sealed container.

Unlike the experimental methods, it is easy to adjust the model's parameters in the theoretical studies and concentrate on any portion of the cell to monitor thermal behavior. Even though there is a slight discrepancy with real-world conditions, most researchers use numerical methods [8]. Generally, a theoretical model consists of mathematical relationships and parameters that describe the system and parametrization. Developing a battery thermal model is the initial stage in numerical simulations. These models are combined with Electrochemical and Equivalent Circuit Models (ECMs) to predict heat generation within batteries and enhance the Battery Thermal Management System (BTMS) [9]. The complete development of the cell's electrochemical reactions can be obtained by a set of governing equations for kinetics, transport processes, and energy dissipation in an electrochemical method, which provides the complete formation of electrochemical actions and reactions of the cell. These models are more accurate, but they are complex and time-consuming. They need high-power computing to solve non-linear differential equations, and it is not easy to obtain battery-specific information due to proprietary technology [10,11].

The selection of a realistic model is critical for estimating the State of Charge (SoC); inaccurate determination of SoC will lead to catastrophic situations such as over-discharge or overcharge. Researchers commonly use ECM because it is a simple approach, fast to execute, and makes it easy to analyze and estimate precise SoC, open circuit voltage, and terminal voltage under dynamic loading conditions. This model is also capable of predicting cell temperature. As ECM is easy to program into microcontrollers and ignores the physical aspects of batteries, it is a heuristic method. The ECM uses circuit elements such as voltage sources, resistors, and capacitors [12,13]. The two electric circuit models that fall under the broad category of impedance-based electrical models [14,15] are the run time-based electrical model [16,17] and the Thevenin-based electrical model [18,19]. Impedance-based electrical models are developed by impedance spectrum measurements. Impedance fitting processes are complex and nonintuitive and work only for fixed SoC and temperature. Run time-based models estimate SoC, cell voltage, and thermal behavior using complex network circuits and look-up tables. However, with these models, the accuracy of estimating battery parameters is poor.

A voltage source, resistors, capacitors, and inductors are used in the Thevenin-based model. This model can be directly connected to a different electrical system. Under dynamic conditions, the Thevenin model can estimate the battery voltage's transient response with a load change [20,21]. So, the Thevenin model is proposed for the study in this work. First-order resistance capacitor and second-order resistance capacitor are the two classifications of the Thevenin model widely used for BTMS development and power management control. To evaluate the dynamic behavior of lithium-ion battery performance, a single resistor and a single RC network coupled in series make up the first-order resistance capacitor model [22]. Internal heat generation, cell temperature, internal resistance, voltage, and state of charging parameters are simulated by building a first-order RC model in MATLAB SIMLINK [23]. The second-order resistance capacitor model, known as the dual circuit model, has two RC components connected in series [24].

The first-order Thevenin and second-order Thevenin models can provide a good balance between computational complexity and improved output results. The second order gives more precise output under different operating conditions than the first order. In an Equivalent Circuit Model, R_s, R_1, R_2, C_1, and C_2 represent various electrical properties of the cell. R_s is the ohmic resistance that causes voltage drop proportional to the current drawn, R_1 is the charge transfer resistance (electrolyte resistance), and R_2 is the polarization resistance that happens during charging and discharging. The value of R changes with SoC and load current. A sharp increase in R_s, R_1, and R_2, particularly at higher currents, causes high heat generation. C_1 indicates the electrolyte capacitance, and C_2 involves charge separation at electrode–electrolyte interfaces.

In this work, cell parameters of Lithium Nickel Manganese Cobalt Oxide (NMC) cells such as R_s, R_1, R_2, C_1, and C_2 are calculated experimentally. Using these estimated parameters, an ECM is built to predict the heat generation inside the cells and the terminal voltage of the battery pack at various conditions. With this model, an effective BTMS is built using Raspberry Pi and a liquid cooling system to control the cell temperature within a set range.

2. Experiment Setup and Methodology

This work is divided into two parts. The first part of the work concentrates on building an ECM for the cells. The second part of the study focuses on implementing the ECM in a Raspberry Pi to effectively control the temperature of the cells in a battery module. The cell chosen for this study is a BAK-made, cylindrical form factor 18650, NMC chemistry (Lithium Nickel Manganese Cobalt Oxide) cell. The specifications of the cell are given in Table 1. As per the specifications provided by the manufacturer, the upper and lower limits of the cut-off voltage are 4.2 V and 2.5 V. For this study, we have maintained the lower cut-off voltage to 2.5 V to prevent deep discharge of the cells. Figure 1 shows the experimental setup employed for obtaining the cell parameters. A list of instruments used in the experimental setup is given in Table 2. A 500 mL mineral oil bath with an insulated chamber (isolation box) houses the cell under test. To replicate the ambient conditions, the temperature of the oil bath can be varied or fixed to an operating temperature using a thermal bath. The maximum and minimum operating temperatures that can be maintained in the bath are 120 °C and −10 °C. The flow rate of the mineral oil from the thermal bath to the isolation box can be adjusted within the range of 0.5 to 5 LPM based on the requirement. The flow rate of the mineral oil is measured using a Meg Flow 6410 flow meter with a measuring accuracy of ±1% of the measured value. The heat generated by the cell during the discharge and charging can be found using the oil flow rate and temperature difference between the oil flowing into and out of the isolation box.

Table 1. Lithium-ion cell specifications.

Device	Description
Cell	BAK 840, 18650 Cylindrical Type
Chemistry	NMC
Voltage	4.2 V (peak), 3.6 (nominal)
Current capacity	2.4 Ah
Maximum discharge rate	2 C
Recommended charging rate	1 C

Table 2. List of instruments used in the experimental setup.

Device Name	Instrument Details	Purpose
DC Electronic load	Precision-BK8610	Battery loading
Battery charger	IMAX B6AC	Charging
Flow sensor	Meg Flow 6410	Measure the mineral oil flow
PT 100 sensor	Sensor	To measure the temperatures
Data Logger	Masi bus 85XX	Data logging
Thermal Bath	Heat exchanger	To maintain the temperature

For measuring the cell temperature, PT100 sensors are installed on the surface of the cell at three locations. PT100 is used to measure temperatures of up to 800 °C. The maximum possible error in the case of temperature measurement was calculated from the minimum values of the temperature measured and the indicator's accuracy. The error in the temperature measurement is around 0.05%, which is close to 0.015 °C for the 30 °C temperature measured. Using a Masibus 85XX data acquisition system, all the temperatures,

including the thermal bath and mineral oil flow rate, are acquired and stored in Excel. An electronic load of BK PRECISION 8610 is used in this study to charge and discharge the cell. According to the manufacturer's specification, the voltage and current measured by the BK Precision have an error of 0.05% and 0.025%. The cell is loaded in the isolation box before setting the desired temperature in the thermal bath. Using the software interface, the charging and discharging parameters are recorded in the laptop. To ensure thermal stability, cells are allowed to rest for two hours after each charge and discharge cycle. During the experimentation, the cells are discharged at various C-rates of 0.5 C, 1 C, 1.5 C, and 2 C, and temperatures of 10 °C, 20 °C, 30 °C, and 40 °C, while charging is carried out at a 1 C rating as per the manufacturer's specifications.

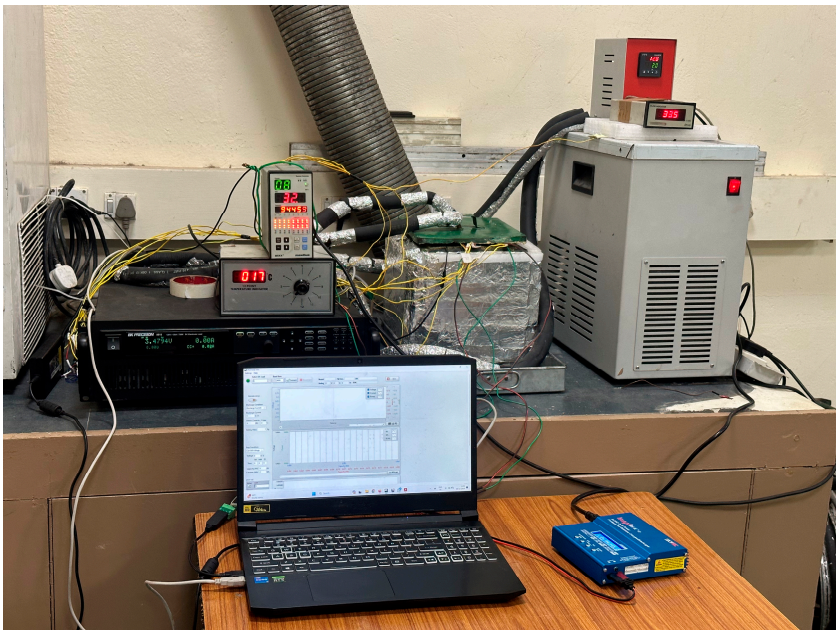


Figure 1. Experimental setup for measuring cell parameters.

2.1. Equivalent Circuit Model (ECM)

This work utilizes a second-order equivalent electrical circuit model to simulate the transient behavior of the cells. As stated earlier, second-order ECM was chosen because it provides a compromise between computational requirements and accuracy [25]. This model goes beyond simpler representations and captures the dynamic voltage response under varying conditions. This model predicts how the batteries' terminal voltage changes with current, temperature, and SoC. This capability makes it valuable for implementation in Battery Management Systems (BMSs) used in electric vehicles and other electronic gadgets that use LIBs. A schematic of the Thevenin second-order Equivalent Circuit Model is shown in Figure 2.

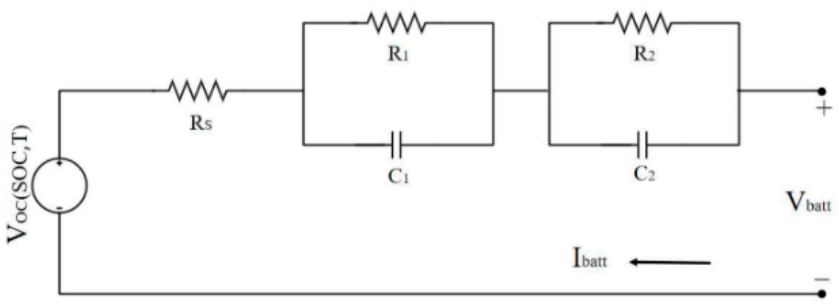


Figure 2. Thevenin model.

Parameters such as resistors R_s, R_1, and R_2 and capacitors C_1 and C_2 depend on the battery's SoC, temperature (T), and current (I). MAT Lab Simulink is used to simulate the Equivalent Circuit Model to predict heat generation. Equations (1)–(8) will be used to determine BTV. The results of the simulation are discussed in the Results and Discussion section.

Applying Kirchhoff's current and voltage laws to Equations (1)–(3) [26,27],

$$I_{batt} = (I_{R_n} + I_{C_n}) \tag{1}$$

$$I_C = \frac{dQ_C}{dt} \tag{2}$$

$$Q_C = V_n \cdot C_n \tag{3}$$

$$\frac{dV_1}{dt} = \frac{V_1}{R_1 c_n} + \frac{I_{batt}}{C_n} \tag{4}$$

$$\frac{dV_2}{dt} = \frac{V_2}{R_2 c_n} + \frac{I_{batt}}{C_n} \tag{5}$$

The integration factor method is used for solving the above differential equations.

$$V_1 = I_{batt} R_1 \left[1 - e^{(-t/R_1 C_1)}\right] + V_1(0) e^{(-t/R_1 C_1)} \tag{6}$$

$$V_2 = I_{batt} R_2 \left[1 - e^{(-t/R_2 C_2)}\right] + V_1(0) e^{(-t/R_2 C_2)} \tag{7}$$

$$OCV = BTV + V_1 + V_2 + I_{batt} R_s \tag{8}$$

V_1 is the voltage drop across R_1 and C_1. V_2 is the voltage drop across R_2 and C_2. I_{batt} is the current, and BTV is the cell or battery terminal voltage. SoC is calculated using the coulomb counting technique, which is given below [18]:

$$SoC = SoC_i - \frac{1}{3600 * Q_{batt}} \int I_{batt}\, dt \tag{9}$$

where SoC_i is initial SoC, Q_{batt} is the capacity of the cell in Ah.

2.2. Model Parameterisation

The pulse discharge technique, commonly known as hybrid pulse power characteristic (HPPC), is used to estimate model parameters. The HPP test is a standard test utilized by researchers to evaluate the batteries used in electric vehicles. Unlike constant current tests, HPP tests use short bursts of current. This approach provides the battery's response to quick changes in power demands. During testing, cell voltage, discharge current, and battery temperature data are continuously recorded with the help of a data logger. With these recorded data, the cell parameters are calculated using Equations (10)–(14). In these equations, V_1, V_2, and V_3 values are obtained by analyzing battery voltage after the discharge pulse, as illustrated in Figure 3.

The resistance R_s is calculated using Equation (10) [25]. This equation requires the magnitude of the current pulse discharge and the voltage response measured one second after the discharge pulse.

$$R_S = \frac{V_o - V_1}{I} \tag{10}$$

The resistance R_1 is calculated using Equation (11) [25], which takes into account the battery's voltage response at the tenth second after the discharge current pulse and the magnitude of the discharge current pulse, as shown in Figure 3.

$$R_1 = \frac{V_1 - V_2}{I} \tag{11}$$

The resistance R_2 is calculated using Equation (12) [25], using the battery's voltage response after eighteen seconds, as shown in Figure 3.

$$R_2 = \frac{V_2 - V_3}{I} \tag{12}$$

The capacitance of C_1 and C_2 can be estimated by the following equations [25].

$$C_1 = \frac{9I}{(V_2 - V_1) ln \frac{V_2}{V_1}} \tag{13}$$

$$C_2 = \frac{8I}{(V_3 - V_2) ln \frac{V_3}{V_2}} \tag{14}$$

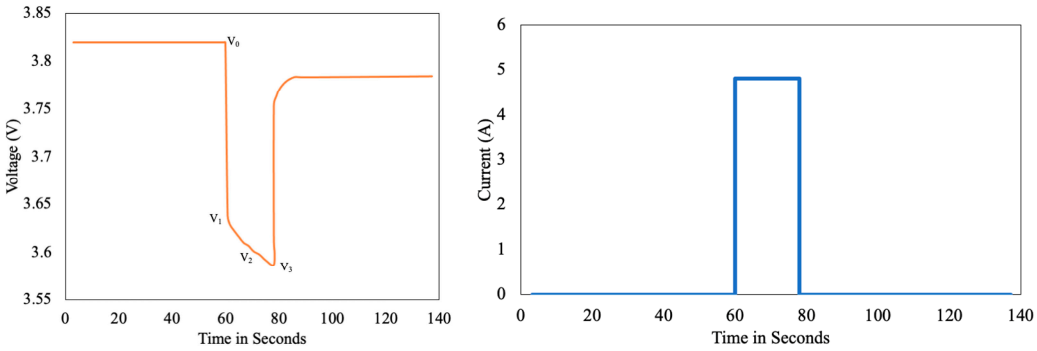


Figure 3. Variation in voltage and current pulse with time.

2.3. Thermal Modeling

ECM parameters depend on SoC and battery temperature. The average cell temperature is determined by taking the battery's skin temperature, which is assumed to be uniform. Battery skin temperature is calculated by solving the lumped capacitance equation, as shown below, where m represents the mass of the battery, C_P represents specific heat capacity, T represents the skin temperature of the battery, h represents the heat transfer coefficient, T_{amb} represents ambient temperature, A_{batt} represents the surface area of the battery, and $\dot{Q}$ represents the heat generation rate. Equation (15) is employed to calculate $\dot{Q}$, and to make the calculations simple, reversible heat is avoided.

$$mC_P \frac{dT}{dt} = h\ A_{batt}(\mathrm{T} - T_{amb}) = \dot{Q} \tag{15}$$

$$\dot{Q} = I^2_{(batt)} \left(R_S + R_1 + R_2 \right) \tag{16}$$

2.4. Open Circuit Voltage

The voltage across the battery terminals under no load conditions is known as open circuit voltage (OCV), and it changes with cell capacity during charging and discharging. For LIBs, it has a non-linear relation with SoC, making OCV crucial for accurate modeling. To determine the OCV, extensive experimental trials are conducted on the cells by subjecting them to charging and discharging cycles at various C ratings and temperatures as defined in Section 2. Equation (17), as explained by Zhang, et al., 2018 [28], shows a typical OCV-SoC relationship obtained by fitting a polynomial curve to the experimental data concerning the temperature variation. S is the SoC value, VOC is the battery open circuit voltage under various operating temperatures, and a_1, b_1, a_2, b_2, and c are the coefficients for the temperature.

$$V_{OCV} = a_1\ e^{b_1\ S} + a_2\ e^{b_1\ S} + C\ S^2 \tag{17}$$

The plotted OCV data with 10% SoC resolution after the cell was charged and discharged at 0.5 C at 30 °C are shown in Figure 4. The figure has both the charging and discharging curves represented in a single chart. The green line shows the discharging trend, starting from 100% SoC and ending at 10% SoC (lower cut-off voltage as prescribed by the manufacturer). If OCV, V_1, V_2 and $I_{batt}R_s$ are known, BTV can be determined theoretically using Equation (8).

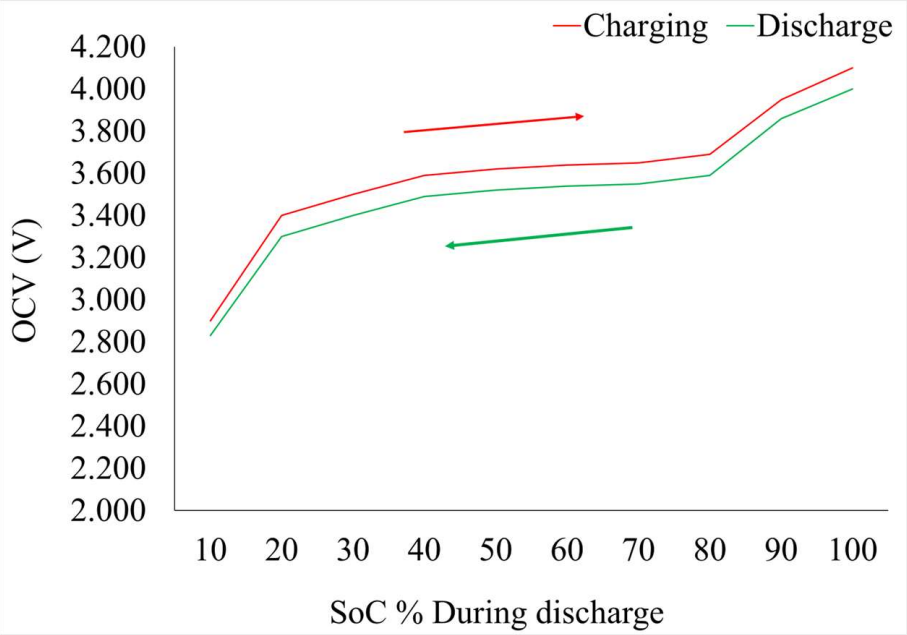


Figure 4. Charging and discharging—open circuit voltage versus SoC.

2.5. ECM-Based Tab—Cooling System

Developing a highly effective cooling system is essential to support high-energy-density cells. Though air cooling and liquid cooling systems are the popular choices for EV battery packs, they are not very effective. Several studies reveal that cell tab cooling is more effective than surface cooling in controlling the cell temperature and aids in improving the cell cycle life [29,30]. Although tab cooling controls the temperature effectively, its implementation is complex as the surface responsible for the energy supply (electricity) also needs to dissipate heat. As a part of previous work, a tab-cooling system is designed and tested to check its effectiveness over surface cooling. The results of that work are presented in another paper [31]. In this paper, the same setup is utilized to check the effectiveness of the cooling system when it is integrated with the Equivalent Circuit Model (ECM)-based cooling system. Figure 5 shows the experimental setup used in this study. The setup has a tab-cooling chamber housing three cells connected in parallel. Only the positive and negative terminals of the cells are cooled instead of cooling the cylindrical surface of the cells. As the heat generated is low and to obtain a good temperature difference between the inlet and exit of the tab-cooling chamber, a coolant with low specific capacity and dielectric property is required, so mineral oil is used as a coolant in the circuit.

The setup includes a reservoir that is a customized car wiper water storage tank where the mineral oil is stored. When necessary, the coolant can be cooled to a specific temperature by utilizing an AC evaporator coil submerged in the tank. A 12 V DC pump moves the coolant in the system at a desired flow rate. The pump's speed can be adjusted using a DC motor controller with input from the Raspberry Pi board. A heat exchanger is linked between the tab-cooling chamber and the reservoir. Coolant from the reservoir is pushed into the lower chamber of the pack and then flows into the upper chamber of the cells through the loop. After absorbing heat from the cells, the coolant moves to the heat exchanger. Heat is transferred from the coolant to atmospheric air in the heat exchanger.

The setup also has a bypass valve to bypass the heat exchanger when the AC evaporator coil (chiller) is used as a sink.

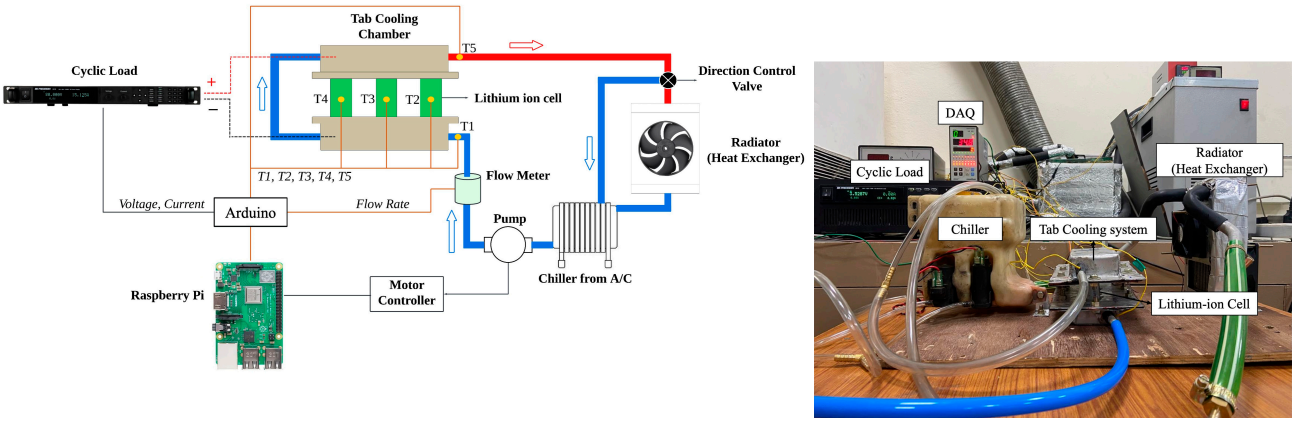


Figure 5. ECM-based tab-cooling system.

A Raspberry Pi is used to control the coolant flow in the system. This involves a Python program that utilizes a predictive algorithm. This algorithm was developed using data collected earlier in the process. To estimate the heat generated during the discharge, =the data containing values of R_s, R_1, R_2, C_1, C_2, and voltage concerning SoC and temperature in the form of polynomial equations are utilized. The data are fed to a regression-based predictive machine learning model to predict voltage, R_s, R_1, R_2, C_1, and C_2 with respect to SoC, discharging current, and temperature. The predictive model was built with Python code that includes the SK learn library, panda library, and NumPy library. The machine learning model used was linear regression with gradient descent as the optimization algorithm to reduce the cost function or mean square error. The learning rate was kept at 0.01 and the number of steps was 100. The model converged with an mse of 0.12. The model had 80% of data for training purposes and 20% for testing purposes, with an accuracy of 83%. This predictive model was fed to Raspberry Pi, which estimated the thermal load using inputs from the current sensor, voltage sensor, and temperature sensors. Figure 6 illustrates the layout of the EMC-based cooling system used in this work.

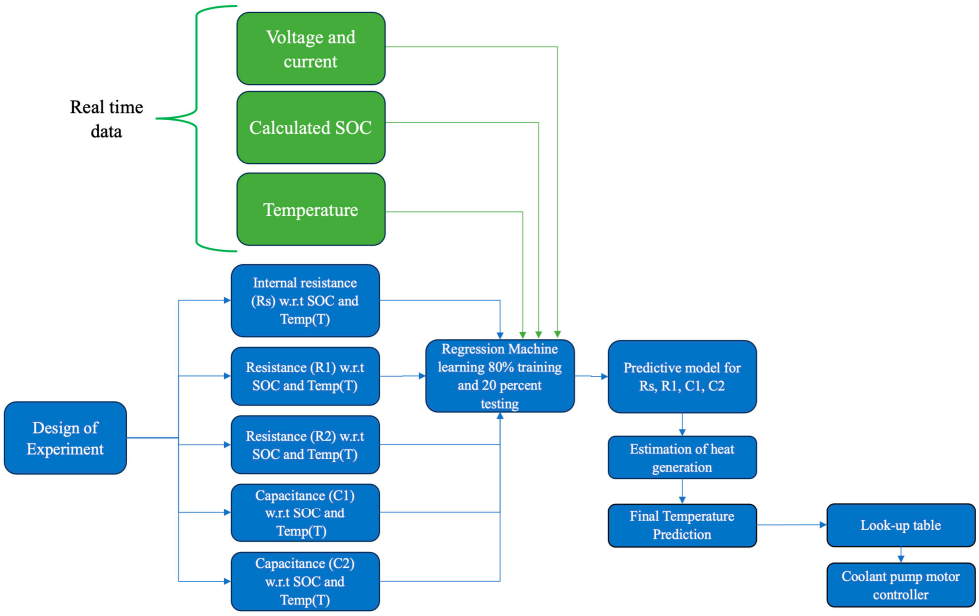


Figure 6. Layout of ECM-based cooling system for battery pack.

3. Results and Discussion

This work aims to improve the performance of a lithium-ion battery pack thermal management system using the cell's ECM. The study concentrates on modeling the lithium-ion cell using the ECM in the first part of the work. The developed model is interfaced with a thermal management system to predict the heat generation from the cell in the second part of the study. The model predicts the heat generation in the cell based on the discharge current, SoC, and ambient temperature and alters the coolant flow rate to maintain the cell temperature. To characterize the cells, the cells are subjected to discharging at various ambient conditions. The results are obtained explicitly for 16850 NMC cells at 0.5 C, 1 C, and 2 C discharge rates and 10, 20, 30, and 40 °C temperatures. The initial phase focuses on cell parameterization, cell voltage, and heat generation findings. The subsequent phase provides an overview of the results of implementing the ECM-based thermal management system.

3.1. Cell Parameterization

When a cell at full charge is drained at a higher C rating, the voltage is not constant and instantly reduces due to ohmic resistance (R_s). As mentioned in Section 2.2, R_s is calculated using Equation (10). Figure 7a shows the plot of the calculated R_s values estimated at a 1 C discharge rate and different temperatures. From the plot, the R_s values are reasonably constant between 70 and 30% of SoC during discharge conditions. When the cells are maintained at 10, 20, 30, and 40 °C, Rs values are 46, 32, 24, and 14.9 mΩ, respectively, for 30% SoC. With respect to the operating temperature, the ohmic resistance values are higher at lower operating temperatures due to a reduction in the diffusion rate at the cathode and anode and slowdown of the electrochemical reactions. When the battery operates at 20 °C with 20, 40, 60, and 80% of SoC, the R_s values are 30.5, 29.5, 28, and 27 mΩ, respectively. It is also understood that Rs values are higher at lower SoC values due to higher internal resistance and irreversible heat generation. The trends of R_1 and R_2 are similar to R_s. R_1 is calculated using Equation (11). Figure 7b shows the plot of R_1 at various temperatures, estimated at a 1 C discharge rate. From the plot, it is understood that the slope of R_1 does not vary much between 40 and 70% of SoC, and when the cells are discharged to less than 30% of SoC, R_1 values increase exponentially. R_2 is calculated using Equation (12). Figure 7c shows the plot of R_2 at various temperatures estimated at a 1 C discharge rate. Similar to R_1, the slope of R_2 remains constant between 40 and 90% of SoC. When the cells are discharged to less than 40% of SoC, R_2 values increase exponentially. R_s, R_1, and R_2 values are high at lower SoCs due to slow mass transport and diffusion limitations [32].

As mentioned in Section 2.2, C_1 is calculated using Equation (13). Figure 7d shows the plot of C_1 at various temperatures estimated at a 1 C discharge rate. The plot shows that the slope of C1 does not vary much between 80 and 100% SoC. When the cells are discharged to less than 30% of SoC, C_1 values are reduced drastically due to the limitation of the diffusion process. When cell temperatures are 10, 20, 30, and 40 °C at 30% of SoC, C_1 values are 1.7, 2.3, 2, 5, and 2.65 kF, respectively. It is also noted that C_1 values are high at higher operating temperatures. C_2 is calculated using Equation (14). Figure 7e shows the plot of calculated C_2 values estimated at a 1 C discharge rate and various temperatures. Like C_1, C_2 values are high at higher operating temperatures but have an opposite trend. When the cells operate at 20, 40, 60, 80, and 100% of SoC at 20 °C, C_2 values are 38, 45, 71, 49, and 94 kF, respectively. This confirms that C_1 and C_2 values increase when the temperature is increased. C_2 values increase and reduce throughout the SoC due to the dynamic character of capacitance [32,33].

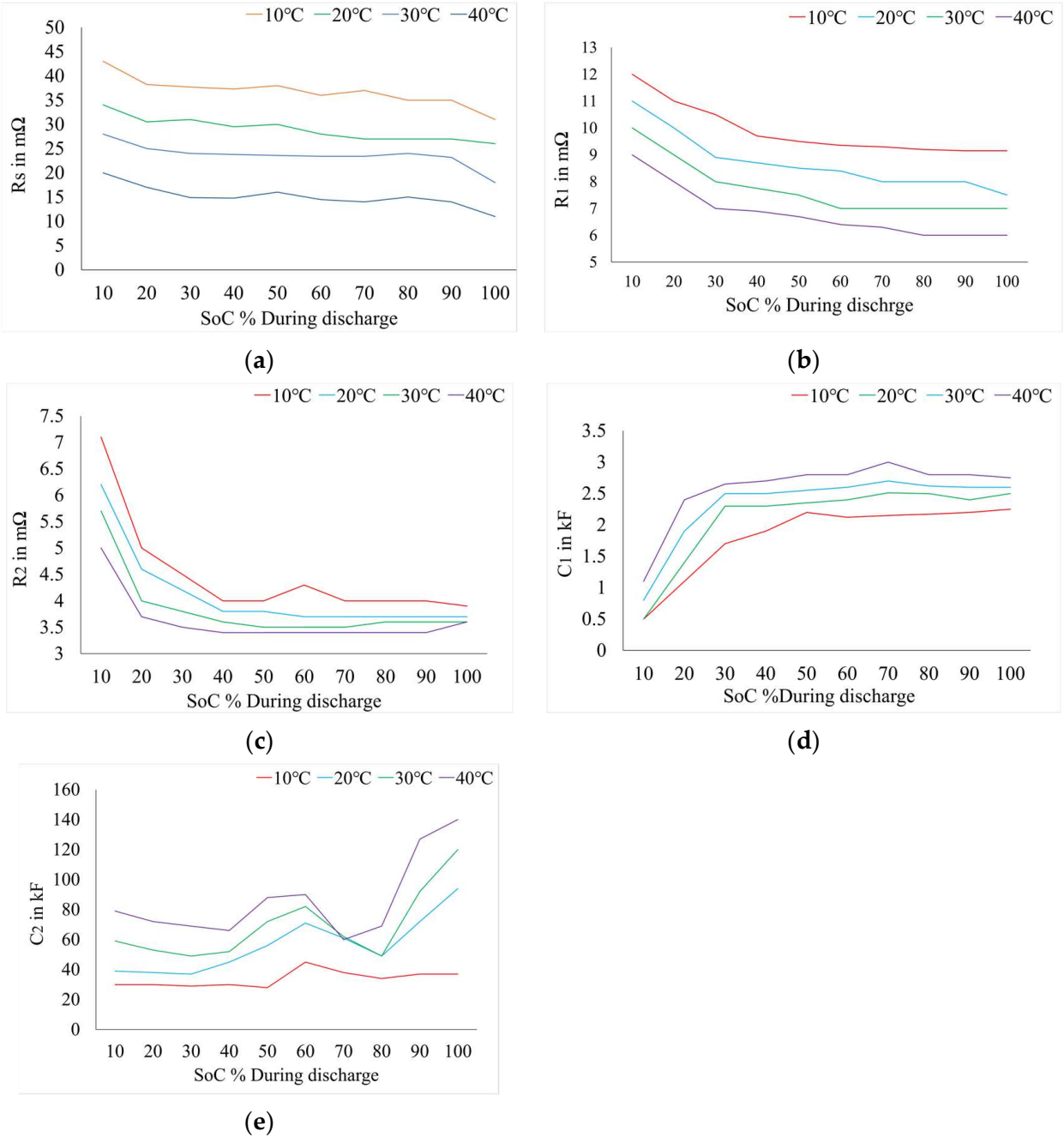


Figure 7. (**a**–**e**) Plots of the calculated cell parameters at the 1 C discharge condition.

3.2. Battery Voltage

Figure 8a shows the battery voltage profile during cell discharging at 0.5 C, 1 C, and 2 C at a 30 °C temperature. The voltage profile confirms that during 0.5 C, 1 C, and 2 C ratings, at the beginning of the battery discharge (until 80% of SoC), battery voltage dropped drastically due to higher ohmic resistance, activation losses, and mass transport losses [34]. Figure 8b–d compare the voltage profiles with the experimental and theoretical values obtained at 0.5 C, 1 C, and 2 C, respectively. At a 30 °C temperature, the measured cell voltage at 50% of SoC and 0.5 C, 1 C, and 2 C was 3.4 V, 3.24 V, and 3.1 V, respectively, whereas the estimated cell voltage at the same condition was around 3.45 V, 3.28 V, and 3.06 V, respectively. The maximum error in the measurement is around ±4%. A comparison of experimental and theoretical voltage data confirms that the developed model can predict cell voltage with better accuracy.

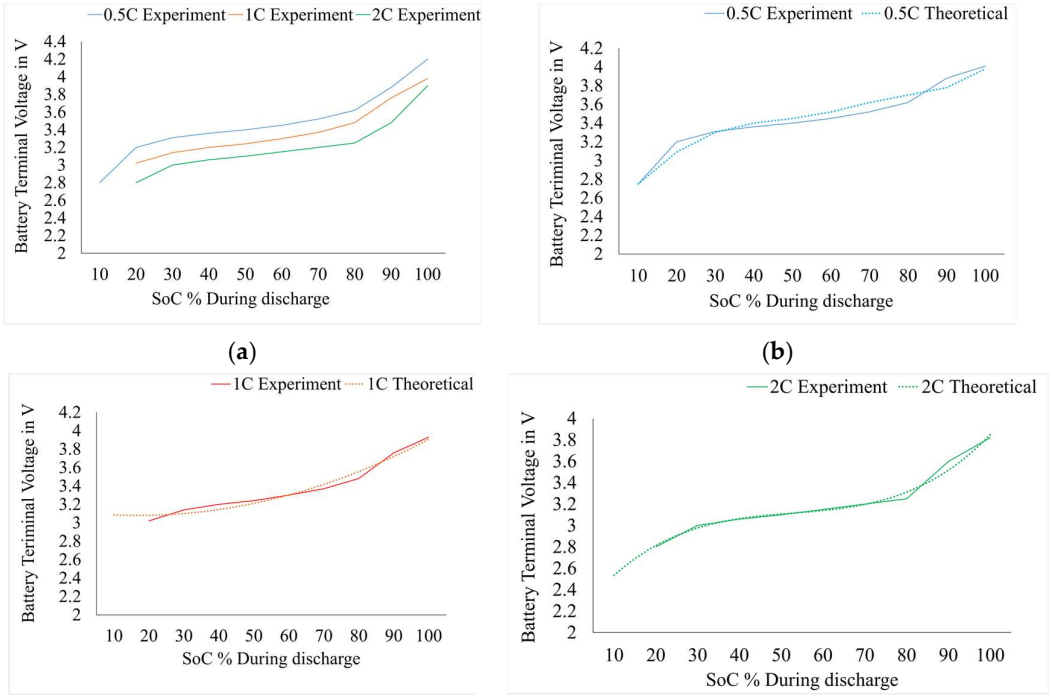


Figure 8. (**a**–**d**) Experimental and calculated battery terminal voltage during discharging at 0.5 C, 1 C, and 2 C at 30 °C.

3.3. Heat Generation Rate

The heat generation in the cell during the discharge is calculated using the conservation of energy principle; that is, the energy released by the cell is transferred to the mineral oil that is circulated. Experimentally, heat generation can be calculated by considering the temperature variance, flow rate, and specific heat capacity of the oil. Theoretical heat generation is calculated by using Equation (16). Figure 9a shows the battery heat generation profile during the discharging at 0.5, 1 C, and 2 C at 30 °C. The heat generation rates at 10% of SoC are 0.6, 1.5, and 3 W, respectively. The results confirm that beyond a 1 C rating, the heat generation rate increases due to joule heating, which is the dominating factor [34]. It is also observed that the heat generation rate reaches a maximum at the end of the discharge. Figures 9b, 9c and 9d show the comparison of experimental and theoretical heat generation profiles at 0.5, 1, and 2 C, respectively. The measured heat generation at 0.5, 1, and 2 C, at 50% of SoC, was 0.12, 0.16, and 0.5 W, respectively, while the estimated heat generation at the same conditions was 0.121, 0.165, and 0.54 W, respectively. The R^2 values for 0.5 C, 1 C, and 2 C were 0.99, 0.984, and 0.986, respectively.

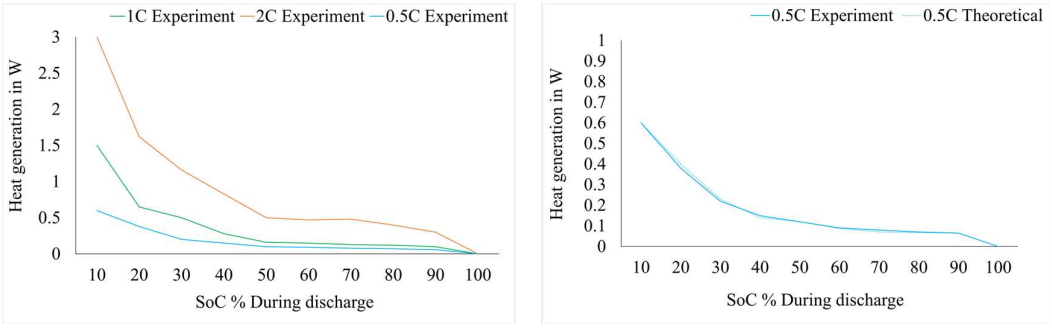
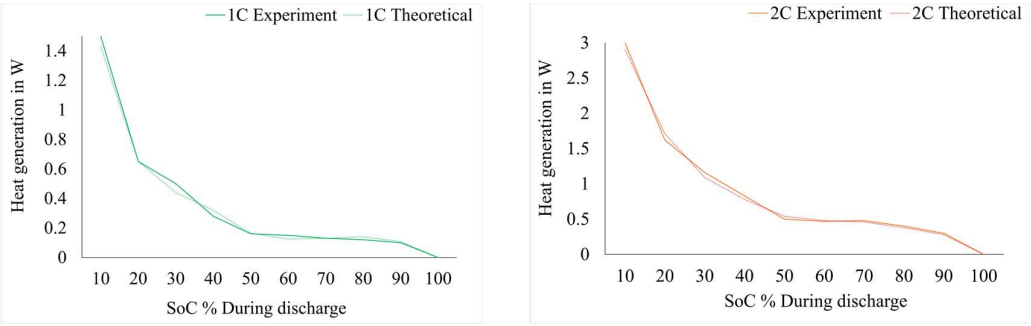


Figure 9. *Cont.*



(**c**) (**d**)

Figure 9. (**a**–**d**) Experimental and calculated heat generation upon discharging at 0.5 C, 1 C, and 2 C at 30 °C.

3.4. ECM-Based Thermal Management System

The second part of this work is dedicated to implementing ECM-based thermal management systems and conducting subsequent experimental trials to showcase their benefits over conventional fixed-flow cooling systems. Figure 10 shows the performance of a liquid-to-air compact heat exchanger, which is part of the ECM-based tab-cooling system, as shown in Figure 5. The heat exchanger is calibrated at various temperatures from 25 to 50 °C in a climate chamber. The calibration is carried out with mineral oil at different flow rates from 0.5 to 3 LPM using a thermal bath with air velocity ranging from 1 CFM to 10 CFM. The calculated specific dissipation (SD) is plotted with respect to the mineral oil flow rate in Figure 10. Specific dissipation represents the ratio between heat rejected by the heat exchanger and the temperature difference between the inlet of mineral oil and the air inlet (climate chamber temperature or ambient temperature). Using the information from the chart given in Figure 10 (for 40 °C ambient temperature), the flow rate of the coolant can be altered to the required rate. Parallelly, the coolant pump is also calibrated with a flow meter to obtain the voltage vs. flowrate profile using the experimental setup shown in Figure 5, and these data are fed into the Raspberry Pi. If Q is the heat generated in the cell or the battery (which is calculated theoretically using Equation (16)), Ts is the temperature of the cell to be maintained, and T_{amb} is the ambient temperature, the thermal resistance is given by $Q/(T_s - T_{amb})$. Once the specific dissipation is calculated, the corresponding mineral oil flow rate can be estimated. Cell temperature can be maintained with these data by activating the required oil flow rate. This leads to significant energy savings when compared to the conventional cooling system.

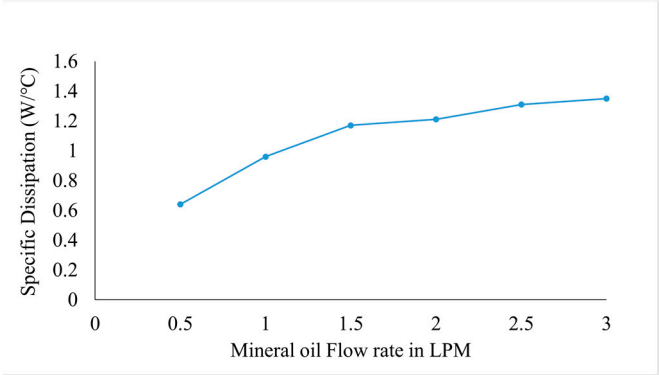
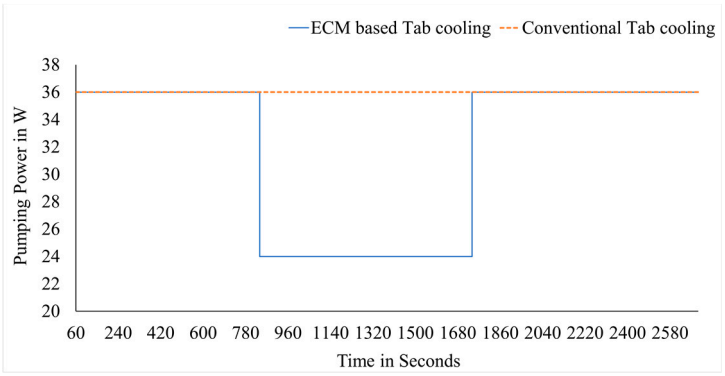


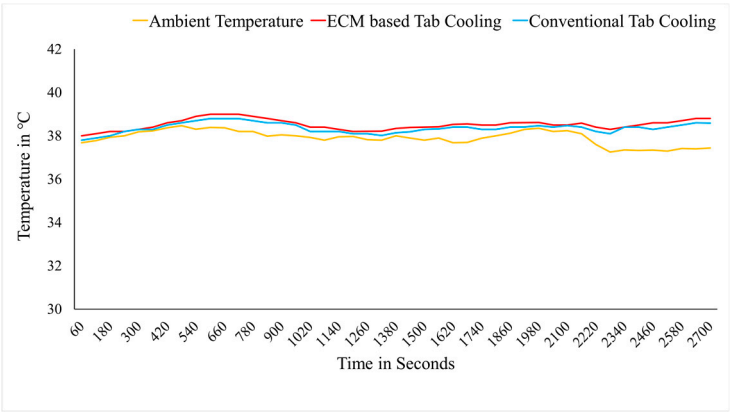
Figure 10. Plot of the calibration of the heat exchanger.

Experimental trials were conducted on the setup with and without the ECM-based cooling system to examine the merits of the ECM-based tab-cooling system over the conventional cooling system (constant flow). Initial tests were carried out using a conventional cooling system approach, with the fixed flow rate set at 2 LPM (the pump was directly

linked to the voltage source). The cell's load current is programmed on the electronic load for 45 min (2 C for 15 min, followed by 1 C for 15 min, and 2.5 C for the last 15 min). The radiator fan was operated at its maximum flow rate of 10 CFM. Cell temperatures, coolant pumping power, and radiator fan power were recorded during the test period. After the conventional cooling system experiments, a Raspberry Pi programmed with a predictive algorithm was integrated into the experimental setup along with the motor controller/driver. Following the Raspberry Pi integration, the ECM algorithm controlled the coolant pump based on voltage, current, and temperature sensor inputs. Tests were then conducted on a modified cooling system under the same conditions as the conventional one. Figure 11a,b show the outcomes of conventional and ECM-based cooling systems. According to Figure 11a, the experimental observations confirm that both the conventional and ECM-based cooling systems maintain a cell temperature close to 38 °C. The operational difference between these two systems is the power consumed to regulate the cell temperature. Figure 11b shows that the conventional cooling system uses around 36 watts to operate both the pump and cooling fan, while the ECM-based system adjusts the flow rate based on the load current. The energy consumption is approximately 36 watts at a load of 2 C, decreases to 24 watts at 1 C, and then rises to 36 watts at 2.5 C. Compared to the standard cooling system, the ECM strategy for controlling the coolant pump resulted in approximately 14% energy savings throughout the experiment. Three more sets of battery packs were made with the same cell chemistry and were tested in the same experimental setup to check the consistency of the results. The results showed no discrepancy with the output. The data was shared as a Supplementary File along with this manuscript.



(**a**)



(**b**)

Figure 11. (**a**) Comparison of performance of the conventional cooling system (**b**) ECM-based tab-cooling system.

4. Conclusions

This study concentrates on building an efficient cooling system for lithium-ion battery packs to reduce the energy consumption of the battery cooling system. Different types of cooling systems are proposed and used by the research community to tackle the thermal runaway issues of the battery pack. This study explores the tab-cooling approach and an Equivalent Circuit Model-based algorithm to control the coolant flow inside the battery pack. The work has two parts: the first part deals with the experimental trials to estimate the cell parameters to build an Equivalent Circuit Model, and the second part of the study concentrates on implementing the ECM along with a predictive algorithm to predict the heat generation in the cell. This study was conducted with BAK-made lithium-ion cells—18650 NMC with 3.7 V and 2400 mAh. The model predicts the heat generation in the cell based on the discharge current, SoC, and ambient temperature and alters the coolant flow rate to maintain the cell temperature. This study confirms that 14% of pumping power can be reduced compared to the conventional constant flow cooling system.

Supplementary Materials: The following supporting information can be downloaded at: https://www.mdpi.com/article/10.3390/vehicles6030057/s1.

Author Contributions: Conceptualization, R.K.C.; methodology, R.K.C.; software, R.K.C.; validation, R.K.C. and M.K.; formal analysis, R.K.C.; investigation, R.K.C. and M.K.; resources, M.K.; data curation, M.K.; writing—original draft preparation, M.K.; writing—review and editing, R.K.C.; visualization, M.K.; supervision, R.K.C.; project administration, M.K. All authors have read and agreed to the published version of the manuscript.

Funding: This research received no external funding.

Data Availability Statement: Data are contained within the article.

Conflicts of Interest: The authors declare no conflict of interest.

Abbreviations

A_{batt}	Battery surface area (m^2)
Ah	Ampere-hour
AC	Air-conditioning system
BTMS	Battery Thermal Management System
BTV	Battery terminal voltage
CFM	Cubic feet per minute
C_p	Specific heat
DC	Direct current
ECM	Equivalent circuit model
EV	Electric vehicle
h	Heat transfer coefficient
HEV	Hybrid Electric Vehicle
HPPC	Hybrid pulse power characteristic
I_{batt}	Battery current (A)
kF	Kilo Farad
LIB	Lithium-ion battery
LPM	Liter per minute
RC	Resistance capacitance
R_s	Ohmic resistance
T	Surface/skin temperature
T_{amb}	Ambient temperature
m	Mass flow rate
mAh	Milli ampere
mΩ	Milli Ohms
NMC	Nickel Manganese Cobalt
V	Voltage
OCV	Open circuit voltage

Q	Heat rejection
$\dot{Q}$	Convection heat generation rate
Q_{Batt}	Battery cell capacity
S	SoC value
SD	Specific dissipation
SoC	State of Charge
V_{batt}	Battery terminal voltage
V_{ocv}	Open circuit voltage
a_1, a_2	Coefficients for temperature
b_1, b_2	Coefficient for temperature
0.5 C, 1 C, 2 C	Battery charging rates
R_1, R_2 and R_n	Transient resistance parameters
C_1, C_2 and C_n	Transient capacitance parameters
V_0, V_1, V_2, V_3 and V_n	Transient voltage parameters

References

1. Jadun, P.; McMillan, C.; Steinberg, D.; Muratori, M.; Vimmerstedt, L.; Mai, T. *Electrification Futures Study: End-Use Electric Technology Cost and Performance Projections through 2050*; NREL/TP-6A20-70485; National Renewable Energy Lab. (NREL): Golden, CO, USA, 2017; p. 94.
2. Goodenough, J.B.; Kim, Y. Challenges for Rechargeable Li Batteries. *Chem. Mater. Rev.* **2010**, *22*, 587–603. [CrossRef]
3. Nishi, Y. Lithium ion secondary batteries: Past 10 yearsand the future. *J. Power Sources* **2001**, *100*, 101–106. [CrossRef]
4. Lu, L.; Han, X.; Li, J.; Hua, J.; Ouyang, M. A review on the key issues for lithium-ion battery management in electric vehicles. *J. Power Sources* **2013**, *226*, 272–288. [CrossRef]
5. Iraola, U.; Aizpuru, I.; Gorrotxategi, L.; Segade, J.M.C.; Larrazabal, A.E.; Gil, I. Influence of voltage balancing on the temperature distribution of a Li-ion battery module. *IEEE Trans. Energy Convers.* **2015**, *30*, 507–514. [CrossRef]
6. Hoh, M.; Fuhr, J. Thermal Management of Hybrid Vehicles Battery Systems. In Proceedings of the 24th International Battery, Hybrid and Fuel Cell Electric Vehicle Symposium & Exhibition 2009 (EVS 24), Stavanger, Norway, 13–16 May 2009; pp. 1–10.
7. Robinson, J.B.; Darr, J.A.; Eastwood, D.S.; Hinds, G.; Lee, P.D.; Shearing, P.R.; Taiwo, O.O.; Brett, D.J. Non-uniform temperature distribution in Li-ion batteries during discharge—A combined thermal imaging, X-ray micro-tomography and electrochemical impedance approach. *J. Power Sources* **2014**, *252*, 51–57. [CrossRef]
8. Liu, H.; Wei, Z.; He, W.; Zhao, J. Thermal issues about Li-ion batteries and recent progress in battery thermal management systems: A review. *Energy Convers. Manag.* **2017**, *150*, 304–330. [CrossRef]
9. Gu, W.B.; Wang, C.Y. Thermal-electrochemical modeling of battery systems. *J. Electrochem. Soc.* **2000**, *147*, 2910–2922. [CrossRef]
10. Newman, J.; Thomas, K.E.; Hafezi, H.; Wheeler, D.R. Modeling of lithium-ion batteries. *J. Power Sources* **2003**, *119–121*, 838–843. [CrossRef]
11. Jiang, J.; Ruan, H.; Sun, B.; Zhang, W.; Gao, W.; Zhang, L. A reduced low-temperature electro-thermal coupled model for lithium-ion batteries. *Appl. Energy* **2016**, *177*, 804–816. [CrossRef]
12. Seaman, A.; Dao, T.S.; McPhee, J. A survey of mathematics-based equivalent-circuit and electrochemical battery models for hybrid and electric vehicle simulation. *J. Power Sources* **2014**, *256*, 410–423. [CrossRef]
13. Chan, H.L.; Sutanto, D. A New Battery Model for use withBattery Energy Storage Systems and Electric Vehicles Power Systems. In Proceedings of the 2000 IEEE Power Engineering Society Winter Meeting, Singapore, 23–27 January 2000; Volume 1, pp. e470–e475.
14. Buller, S.; Thele, M.; Doncker, R.W.D.; Karden, E. Impedance-based simulation models of supercapacitors and Li-ion batteries for power electronic applications. *IEEE Trans. Ind. Appl.* **2005**, *41*, 742–747. [CrossRef]
15. Rodrigues, S.; Munichandraiah, N.; Shukla, A.K. A review of state-of-charge indication of batteries by means ofac impedance measurements. *J. Power Sources* **2000**, *87*, 12–20. [CrossRef]
16. Benini, L.; Castelli, G.; Macci, A.; Macci, E.; Poncino, M.; Scarsi, R. Discrete-time battery models for system-level low-power design. *IEEE Trans. VLSI Syst.* **2001**, *9*, 630–640. [CrossRef]
17. Baudry, P.; Neri, M.; Gueguen, M.; Lonchampt, G. Electro-thermal modeling of polymer lithium batteries for starting period and pulse power. *J. Power Sources* **1995**, *54*, 393–396. [CrossRef]
18. Saurabh, S.; Raman, S.R.; Saritha, B.; John, V. A Novel Approach for Electrical Circuit Modeling of Li-Ion Battery for Predicting the Steady-State and Dynamic I–V Characteristics. *Publication* **2016**, *41*, 479–487.
19. Hentunen, A.; Lehmuspelto, T.; Suomela, J. Time-Domain Parameter Extraction Method for Thevenin-Equivalent Circuit Battery Models. *IEEE Trans. Energy Convers.* **2014**, *29*, 558–566. [CrossRef]
20. Johnson, V.H. Battery performance models in ADVISOR. *J. Power Sources* **2002**, *110*, 321–329. [CrossRef]
21. Bobobee, E.D.; Wang, S.; Zou, C.; Takyi-Aninakwa, P.; Zhou, H. Emmanuel Appiah State of charge estimation of ternary lithium-ion batteries at variable ambient temperatures. *Int. J. Electrochem. Sci.* **2023**, *18*, 100062. [CrossRef]
22. Chiang, Y.-H.; Sean, W.-Y.; Ke, J.-C. Online estimation of internal resistance and open-circuit voltage of lithium-ion batteries in electric vehicles. *J. Power Sources* **2011**, *196*, 3921–3932. [CrossRef]

23. Panchal, S.; Dincer, I.; Agelin-Chaab, M.; Fraser, R.; Fowler, M. Experimental and simulated temperature variations in a LiFePO4-20 Ah battery during discharge process. *Appl. Energy* **2016**, *180*, 504–515. [CrossRef]
24. Du, J.; Liu, Z.; Wang, Y.; Wen, C. An adaptive sliding mode observer for lithium-ion battery state of charge and state of health estimation in electric vehicles. *Control. Eng. Pract.* **2016**, *54*, 81–90. [CrossRef]
25. Madani, S.S.; Schaltz, E.; Kær, S.K. An Electrical Equivalent Circuit Model of a Lithium Titanate OxideBattery. *Batteries* **2019**, *5*, 31. [CrossRef]
26. Rajchapanupat, N.; Poramapojana, P. A comparative study of equivalent circuit models for a Li-ionbattery pack of an electric Tuk-Tuk. *IOP Conf. Ser. Mater. Sci. Eng.* **2021**, *1137*, 012014. [CrossRef]
27. Jin, Y.; Li, Z.; Liu, B.; Liu, L. Modeling and simulation of lithium ion battery cosidering the effect of charge and discharge rate. *J. Phys. Conf. Ser.* **2021**, *1907*, 012003. [CrossRef]
28. Xia, R.Z.B.; Li, B.; Cao, L.; Lai, Y.; Zheng, W.; Wang, H.; Wang, W.; Wang, M. A Study on the Open Circuit Voltag and State of Charge Characterization of High Capacity Lithium-Ion Battery Under Different Temperature. *Energies* **2018**, *11*, 2408. [CrossRef]
29. Hunt, I.A.; Zhao, Y.; Patel, Y.; Offer, G.J. Surface cooling causes accelerated degradation compared to tab cooling for lithium-ion pouch cells. *J. Electrochem. Soc.* **2016**, *163*, A1846. [CrossRef]
30. Wang, H.; Li, H.; Ji, Z.; Yang, Z.; Jiang, C.; Lin, H. Cooling the electrode tabs with air to manage the heat transferred through the collectors in traction battery. *J. Energy Storage* **2022**, *48*, 103982. [CrossRef]
31. Muthukrishnan, K.; Kumar, C.R. Study on the effect of tab cooling on the lithium-ion battery pack life cycle. *Arch. Thermodyn.* **2024**, *45*, 291–299. [CrossRef]
32. Hossain, M.; Saha, S.; Haque, M.E.; Arif, M.T.; Oo, A.M.T. A Parameter Extraction Method for the Thevenin Equivalent Circuit Model of Li-ion Batteries. In Proceedings of the 2019 IEEE Industry Applications Society Annual Meeting, Baltimore, MD, USA, 29 September–3 October 2019; ISBN 978-1-5386-4539.
33. Thanagasundram, S.; Arunachala, R.; Makinejad, K.; Teutsch, T.; Jossen, A. A Cell Level Model for Battery Simulation. In Proceedings of the European Electric Vehicle Congress, Brussels, Belgium, 20–22 November 2012.
34. He, K.; Xiong, Y.; Zhang, C.; Dou, Z.; Lin, S.; Li, C.; Sun, Y. An Investigation on the Electrochemical and Thermal Characteristics of$LiMn_{0.6}Fe_{0.4}PO_4/LiNi_{0.5}Co_{0.2}Mn_{0.3}O_2$ Composite Cathode Materials for Lithium-Ion Batteries in Different Health States. *J. Electrochem. Soc.* **2023**, *170*, 090501. [CrossRef]

Disclaimer/Publisher's Note: The statements, opinions and data contained in all publications are solely those of the individual author(s) and contributor(s) and not of MDPI and/or the editor(s). MDPI and/or the editor(s) disclaim responsibility for any injury to people or property resulting from any ideas, methods, instructions or products referred to in the content.